

3D Printing of Complex Wire Geometries for Tailored Resistance Response

Tim Phillips*, Jared Allison*, Joseph Beaman*

*Department of Mechanical Engineering, University of Texas at Austin, TX 78712

Abstract

Additive manufacturing (AM) is a rapidly growing field that enables production of complex geometries without tooling. AM has gained traction as a method of producing complex electronic circuits not possible using traditional techniques. The method explored in this manuscript involves post-build infiltration of conductive inks into complex channels to create resistive elements with tunable properties. A Polyjet printer is used to enable high-precision multi-material components with custom mechanical properties. Further, the conductive pathway geometry can be designed to achieve different resistive responses. These properties allow for decoupling of the stress-strain response and resistance-strain response to produce custom strain gauges with engineered properties.

Introduction

Additive manufacturing (AM) is the process of building parts by joining material, typically layer-on-layer, directly from CAD data [1]. While the field originated as a means of producing functional prototypes, it has experienced remarkable growth in recent years and today is used in a wide variety of prototyping, tooling, and end-use applications. One growing area of interest is in AM of electronics, enabling complex circuitry not possible with traditional circuit manufacturing methods. The primary hurdle in AM of electronics is achieving a high-resolution conductive pathway within the components. AM has shown tremendous potential to create complex geometries, but integrating conductive materials and circuit elements still poses a challenge. Currently, the most popular techniques of incorporating conductive materials are wire embedding, direct ink writing, aerosol jet printing, and coating with conductive materials.

Wire embedding yields pathways with excellent electrical properties dictated by the embedded wire but are limited to planar or simple surfaces [2]. There is also the issue of connecting the wire to an embedded circuit element, which must be done during the embedding process, such as through laser welding [3] or by clamping between conductive plates also embedded in the part [4].

Direct ink writing involves extruding continuous filament or droplets of an ink. This can be a self-contained process where the ink makes up the entirety of the part [5] or incorporated into another process where a conductive ink is written on a non-conductive substrate [6–8]. Each ink writing step takes place on a planar or simple surface; however, low fidelity 3D pathways can be created by stacking multiple planar extrusions. The out-of-plane resistance is expected to differ from in-plane resistance due to a smaller contact area and potential incomplete bonding between layers. Aerosol jet printing is similar to direct ink-writing, using an aerosolized nanoparticle suspension jetted at the substrate rather than a liquid ink. It has many of the same advantages of

direct ink writing, but is capable of even finer detail; however, this makes it slower at building 3D parts [9,10].

Coating with conductive materials involves direct application of conductive material, such as through screen printing, or creating a preferential plating area during manufacture that is subsequently selectively coated. Coating includes the application of conductive material as well as electroless plating conductive material onto the 3D printed part. Electroless plating has been used to successfully coat copper onto fused filament fabricated (FFF) and stereolithography parts, but so far has only been shown to create simple surface-level conductive pathways [11,12]. Conductive coating has been accomplished by creating channels within a part during manufacture then flooding with a conductive material, such as liquid metal [13] or nanoparticle ink [14]. This paper will utilize the conductive coating process due to the limitations highlighted in other methods of creating conductive pathways.

This paper utilizes the material jetting (MJ) additive manufacturing process, also referred to as Polyjet. This type of AM system builds parts by selectively depositing liquid material droplets then solidifying them using ultraviolet light before building the next layer upon it. One big strength of MJ systems is their ability to deposit multiple materials with discrete or graded interfaces to create multi-material parts. The design complexity afforded by this process is utilized in this paper to create strain gauges with tunable responses to tension and torsion part deformation.

Materials and Methods

Specimens were printed using a Stratasys J750 Digital Anatomy printer using a variety of materials, given in Table 1. Multi-material parts were built with a discrete interface between materials. Two support materials were used: a standard gel-like support and an experimental liquid support. The liquid support was used when building the channels, allowing complex geometries without the challenges of removing the standard gel-type support. After building, parts were manually cleaned of support material via high-pressure water jet.

Specimen renderings are provided in Figure 1. Each specimen consisted of 4 parts: (1) rigid end caps, represented as a blue material in the renderings. (2) flexible gauge section, represented as clear in the renderings, (3) stainless steel pins for resistance measurement attachment, shown as silver circles in the renderings, and (4) a conductive channel that spans the flexible gauge section and connects the steel pins, represented as copper in the renderings. A total of four unique channel designs were created plus an additional design that was a combination of two, creating two distinct channels within the same part. The designs were: (1) a single straight channel, (2) five straight channels, connected within the rigid end caps to form one continuous channel, (3) a single helical channel, (4) a 3D stepped channel that only moved in one cardinal direction at a time in a winding pattern, dubbed a “low-poly helix”, and (5) two distinct channels within the same gauge section, a single line and a helix winding around it. The gauge section, defined as the region with flexible material, was nominally 25.4 mm long with a 10.9 x 10.9 mm cross-section, disregarding the void area of the channels. Each channel had nominally a 2 mm diameter. The rigid part has the same cross-section as the flexible part at their interface, then tapers down to a tab for insertion into the tensile testing machine. Path lengths for the conductive traces in each specimen are given in Table 2.

Table 1: Stratasys J750 materials

Material Name	Properties	Purpose
Agilus30	Flexible	Building the flexible portions of the strain gauge
Vero	Rigid	Building the ends of the strain gauge, outside the gauge section
SUP706B	Support	Gel-like support for general purpose building
Model Cleanser*	Support	Liquid support for strain gauge channels

*Model Cleanser is typically only used as a cleanser, but is available as a build material through the GrabCAD Print Beta software package

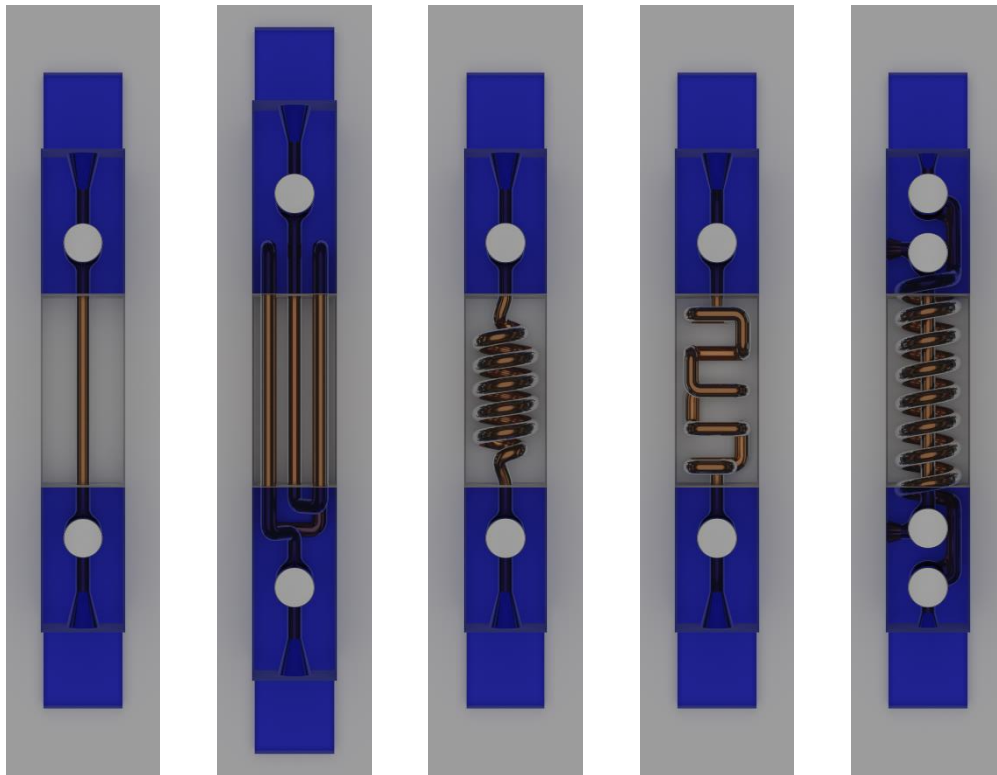


Figure 1: Strain gauge designs featuring (left to right): single line, multi-line, helical, low-poly helical, and dual helical-line channels. The blue material is rigid Vero, clear material is flexible Agilus30, copper material is MG Chemicals 843WB conductive paint, and silver material is stainless steel.

Table 2: Specimen conductive trace lengths

Sample	Gauge Path Length (mm)	Measurement Path Length (mm)
Single-line	25.4	38.1
Multi-line	127.0	221.5
Helix	124.0	136.7
Low-poly helix	122.9	135.6
Dual helix-line	151.6/25.4	206.2/35.6

A water-based conductive paint containing silver-coated copper flakes (MG Chemicals 843WB) was used as the conductive media. It was applied via syringe to push through the strain gauge channel followed by a bolus of air so as to coat the channel with paint while leaving it hollow. Stainless steel pins (PEM TPS) were inserted into the channels prior to coating to create attachment points for resistance measurements. Post-coating, the parts were placed in a vacuum for 4+ hours to accelerate drying. Two coats of paint were used, drying after each coat.

Resistance was measured via an NI myDAQ digital multimeter and recorded via LabVIEW. Measurements were taken every 0.5 s with 0.1 Ohm resolution and a measurement range of 0-200 Ohm.

An Instron 3345 was used to perform extension experiments. A 5 kN load cell was used to measure force and the Instron stage movement was recorded as the strain gauge extension. The test consisted of pulling the specimen 2.5 mm at a rate of 5 mm/min. A picture of the experimental setup is provided in Figure 2. While force was recorded during testing and measured nominally as ~8 N at 2.5 mm extension, stress is not reported. The non-constant cross-section of the gauge section due to the channels, as well as the discrete interface between rigid and flexible material create stress concentrations that make stress calculations non-trivial. Additionally, the focus of this paper is on tailoring resistance response for a given deformation, so the stress-strain response is not explored in this manuscript.

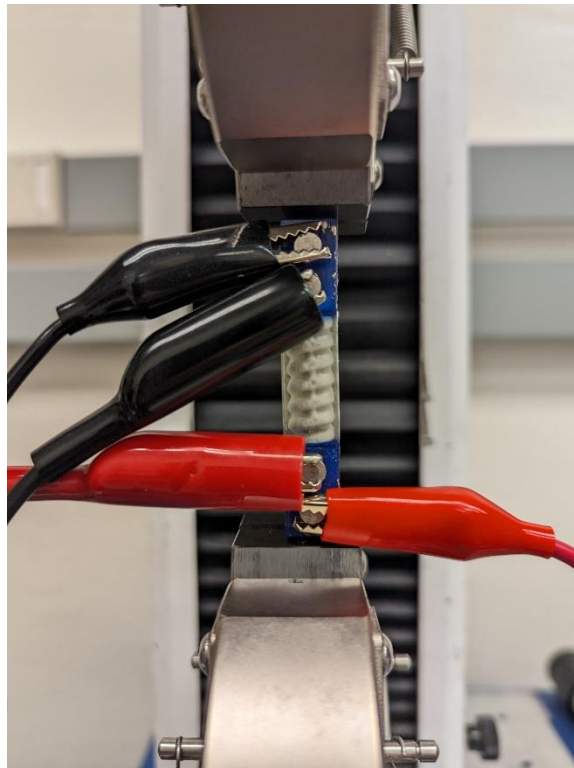


Figure 2: Tensile test resistance measurement setup for the dual-channel specimen.

A custom rotation rig, shown in Figure 3, was used to measure the resistance response of the samples under torsion. The rotation rig was manually operated, so it was not possible to torque

the samples in a smooth, continuous fashion. Instead, each sample was twisted along its central axis positive and negative 90° in 15° increments and held for 15 seconds while the resistance was recorded.

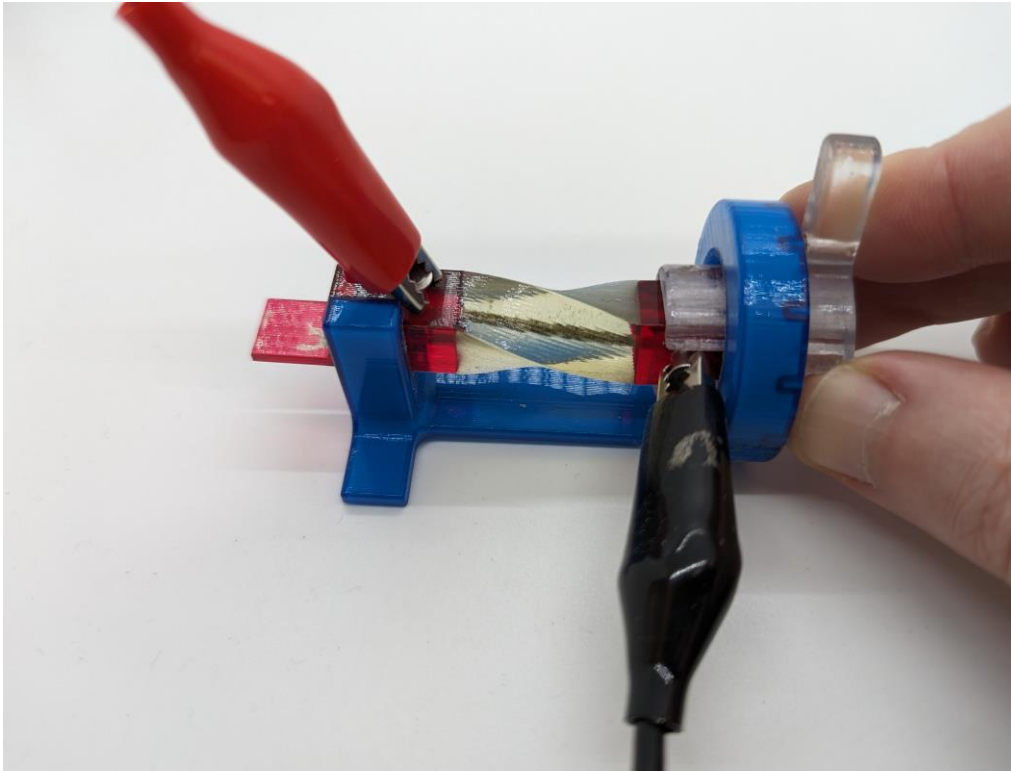


Figure 3: Rotation resistance measurement setup.

Results and Discussion

Tension Response

The resistance response of the strain gauges under tension are given in Figure 4 and Figure 5. As expected, each design exhibited an increase in resistance as the specimen was stretched due to lengthening of the resistive element; however, the absolute value and linearity of the response was dependent on the geometry. At zero extension, the resistance value should be proportional to the measurement path length, with the shortest specimen, single-line, having the lowest resistance and the longest specimen, multi-line, having the highest resistance. This trend was observed; however, the separation between the helical specimens and multi-line specimen was not as great as expected despite the multi-line specimen having a significantly longer measurement path length. One possible explanation for this is that the conductive coating thickness varied between specimens, causing variations in resistance that are independent of measurement path length. Another possibility is that the amount and radius of curvature in the channels has an influence on the resistance.

Best fit lines for the strain responses are provided in Figure 5. The single-line and multi-line designs both exhibited an exponential increase in resistance as they were stretched. The exponential multiplier of the multi-line specimen, 6.40, is approximately 5 times greater than the

multiplier for the single-line specimen, 1.29, the same as the difference in gauge path length. Intuitively, this makes sense as the change in resistance should be proportional to the amount of resistive element being stretched. The helix also exhibited an exponential increase in resistance, though with a much smaller exponential value. The low-poly helix exhibited a more linear response.

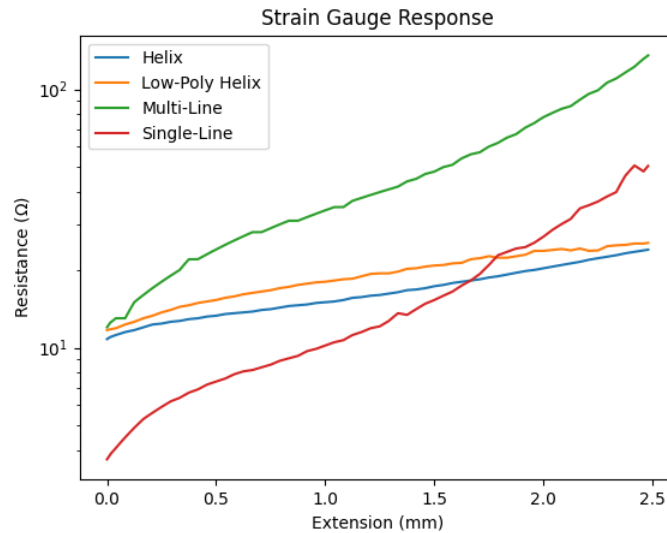


Figure 4: Resistance response for the strain gauge geometries

Three of the dual-channel specimens were printed with the same nominal geometry and tested under the same strain conditions, presented in Figure 6. The general trend of each specimen's longer channel, the helix, having a higher resistance than the shorter channel, the line, remained true. There was some variation, however, when comparing specimens to each other. Specimens 1 and 2 were similar, despite the linear channel in specimen 1 having a stronger response than that of specimen 2, as shown by the steeper slope of the dashed blue line compared with the dashed red line in Figure 6. Specimen 3, however, exhibited a drastically lower response in the helical channel (green solid line), so much so that the resistance of the linear channel (green dashed line) surpassed the helical channel resistance when stretched beyond ~1.0 mm. This response is more inline with what was observed in Figure 4, where the linear channel had a stronger response than the helical channels and had a higher resistance once stretched beyond a certain point. It is unclear whether the variations between these specimens is caused by differences in the coating or manufacturing process and further exploration is needed to determine how to produce more uniform and repeatable specimens.

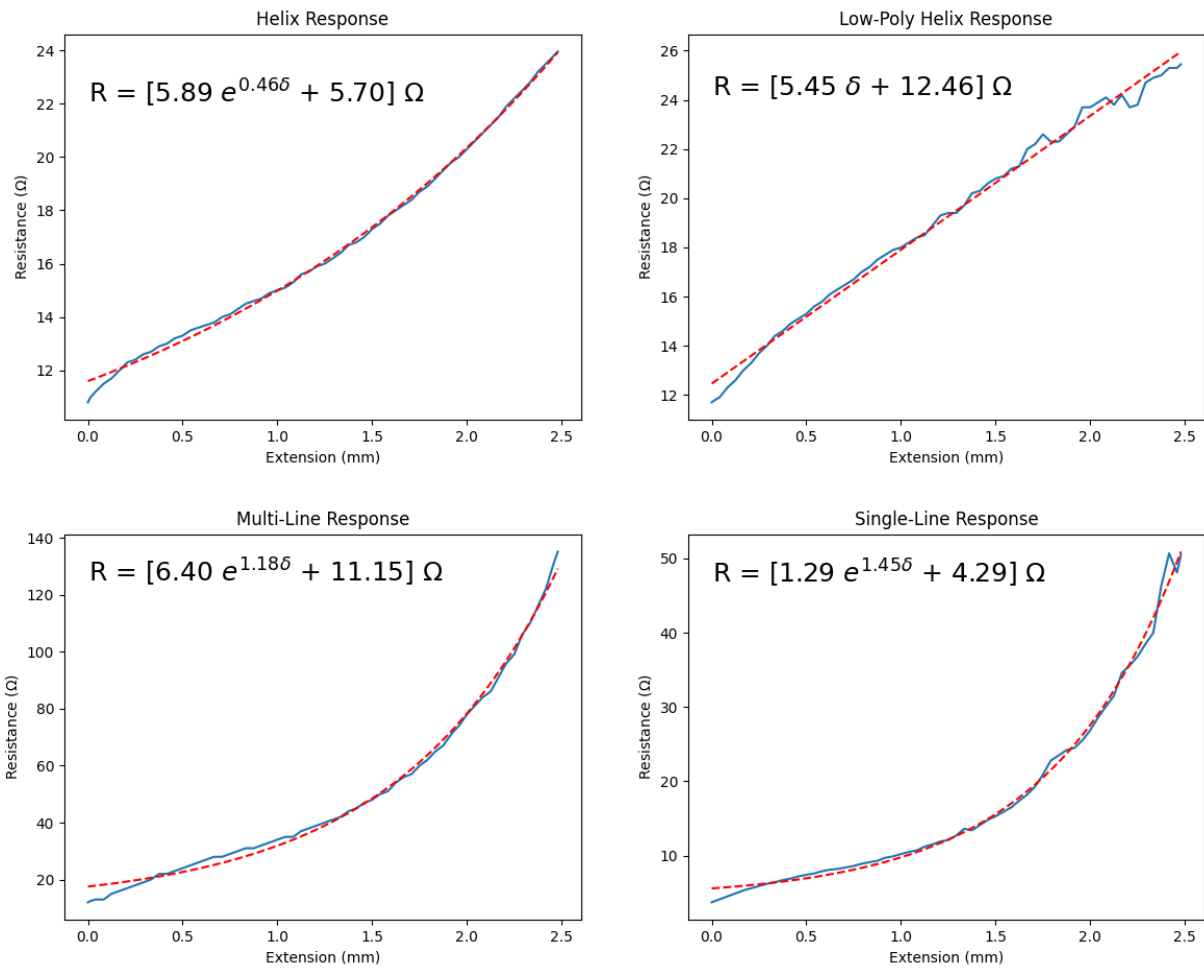


Figure 5: Resistance response of the strain gauges as a function of extension, δ . Experimental data is shown in blue and the best-fit line is overlaid in red dashes with the equation printed on the figure.

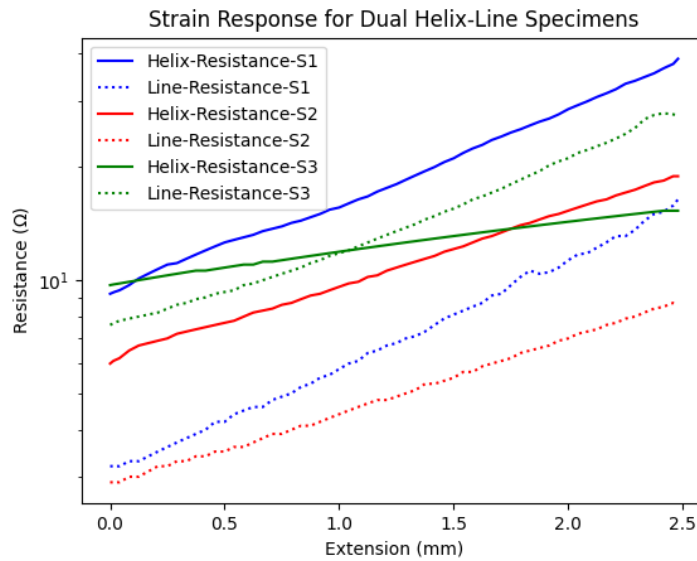


Figure 6: Resistance response under strain for the dual channel helix-line specimens

Torsion Response

After completing the extension experiments, the same samples were used in the rotation test rig. Between successive tests, each specimen was left in a relaxed state for at least 5 minutes, by which point the no-load resistance had returned to the initial level. The torsion response for the single-channel specimens is presented in Figure 7. A positive angle represents rotating the part counter-clockwise, which is aligned with the helix rotation direction. The helix, low-poly helix, and multi-line specimens all exhibit an increase in resistance when rotated in either direction. The multi-line specimen is symmetric within the gauge section, so its resistance response is not expected to be dependent on the direction of rotation, only the absolute value of it. This is true up to a rotation of 60° , but beyond that, counter-clockwise rotation elicits an increased resistance response.

The single-line specimen exhibits little-to-no resistance change regardless of rotation angle. This lack of response is expected since the resistive channel runs through the center of rotation for the torsion test rig, making it so there is no change in path length during rotation.

The dual-channel specimens were tested in the same fashion, their results are presented in Figure 8. The trends found in the single-channel specimens are also found in the dual-channel specimens; the longer helical channel has a higher resistance than the shorter linear channel and only the helical channel exhibits a resistance change when twisted. The resistance values vary significantly between specimens, further confirming that the coating was inconsistent across specimens. The helix in specimen 1 exhibited a significantly stronger response than in the other specimens when rotated counter-clockwise, so much so that rotating beyond 60° resulted in a reading beyond the range of the myDAQ. The test was aborted after 60° as helical data was no longer being recorded, but there was no indication that this affected the linear channel, which continued to show nearly zero change in resistance. This test was repeated and the results were

the same, where rotation beyond 60° resulted in the helical channel resistance going beyond the measurement range.

When released from tension or torsion and allowed to return to their natural state, the resistance of all specimens also returned to the original, un-flexed value. The resistance took a few minutes to return to the original value, likely attributable to the lossy nature of the Agilus30 flexible material used in the gauge section, which also took time to relax back to its natural state.

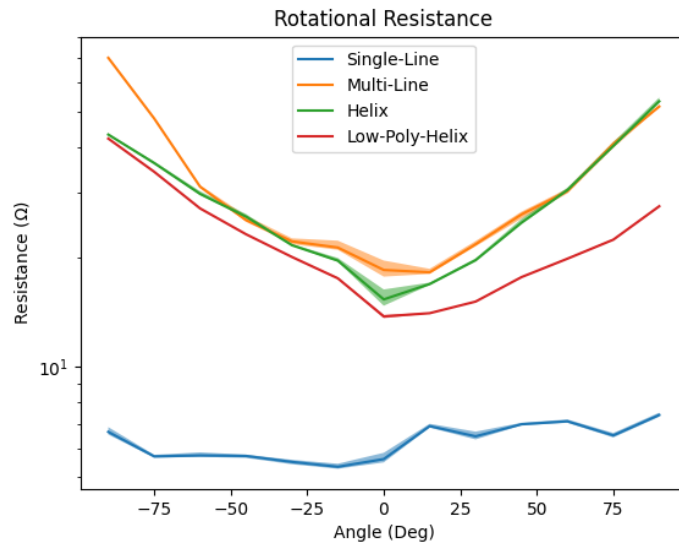


Figure 7: Torsional strain response for single-channel specimens. A positive angle represents a counter-clockwise rotation, along the helical channel direction.

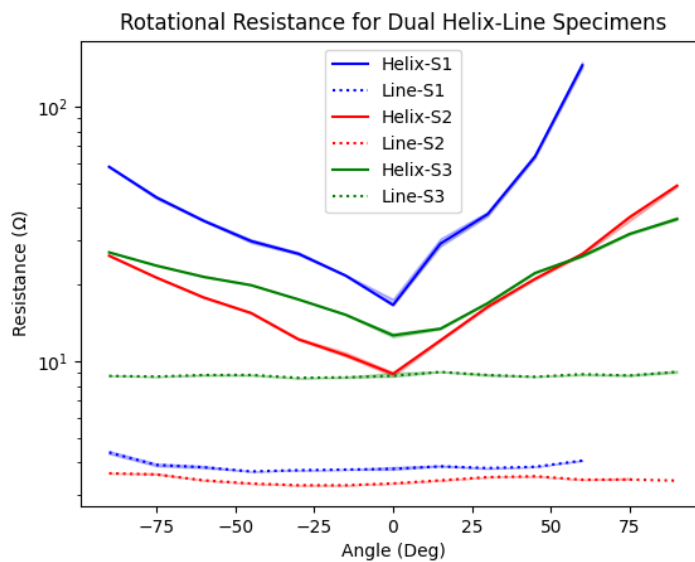


Figure 8: Torsional strain response for the dual-channel Helix-Line specimens. A negative angle represents a counter-clockwise rotation, along the helical channel direction

Conclusion

This manuscript presents a novel low-cost process of creating multi-material 3D printed parts with conductive channels via post-build coating with conductive paint. The resistance of the channels was measured as the specimens underwent tension and torsion testing and showed that the resistance value is related to the channel design and type of part deformation. Based on these findings, it is believed that channels can be designed to achieve specific resistance responses, such as the resistance in a straight channel being unchanged by torsion around the channel axis. This opens the door to multi-element strain gauges that can detect not only the amount, but also the type of deformation the part undergoes. Additionally, it is shown that the conductive coating is capable of bonding to both the 3D printed material as well as the inserted pins, indicating that other circuit elements can be inserted into the parts and connected to the circuit. Potential applications of this include part health monitoring, strain gauges with designed resistance response, and 3D circuitry with embedded circuit elements.

There are a number of next steps identified that would further improve the utility of the process described in this paper. Developing a coating process that is consistent across specimens would improve the useability by making the resistance values predictable and controllable. Testing different materials and graded interfaces would further show the tuneability of the resistance response. Lastly, embedding circuit elements within the polymer substrate mid-build and connecting them with the conductive pathways would open the door for functional electronics beyond strain gauges.

Works Cited

- [1] 2017, *ISO/ASTM52900-15 Standard Terminology for Additive Manufacturing - General Principles - Terminology*, ASTM International, West Conshohocken, PA.
- [2] Billah, K. M. M., Coronel, J. L., Halbig, M. C., Wicker, R. B., and Espalin, D., 2019, "Electrical and Thermal Characterization of 3D Printed Thermoplastic Parts With Embedded Wires for High Current-Carrying Applications," *IEEE Access*, **7**, pp. 18799–18810.
- [3] Espalin, D., Muse, D., MacDonald, E., and Wicker, R., 2014, "3D Printing Multifunctionality: Structures with Electronics," *The International Journal of Advanced Manufacturing Technology*, (72), pp. 963–978.
- [4] Ziervogel, F., Boxberger, L., Bucht, A., and Drossel, W.-G., 2021, "Expansion of the Fused Filament Fabrication (FFF) Process Through Wire Embedding, Automated Cutting, and Electrical Contacting," *IEEE Access*, **9**, pp. 43036–43049.
- [5] Lewis, J. A., 2006, "Direct Ink Writing of 3D Functional Materials," *Advanced functional materials*, **16**(17), pp. 2193–2204.
- [6] Valentine, A. D., Busbee, T. A., Boley, J. W., Raney, J. R., Chortos, A., Kotikian, A., Berrigan, J. D., Durstock, M. F., and Lewis, J. A., 2017, "Hybrid 3D Printing of Soft Electronics," *Advanced Materials*, **29**(40), p. 1703817.
- [7] Williams, N. X., Noyce, S., Cardenas, J. A., Catenacci, M., Wiley, B. J., and Franklin, A. D., 2019, "Silver Nanowire Inks for Direct-Write Electronic Tattoo Applications," *Nanoscale*, **11**(3), pp. 14294–1432.

- [8] Yan, F.-J., Huang, W.-Q., Sang, X.-H., Liang, J.-G., Wan, X., Shao, F., and Gu, X.-F., 2021, "Direct Ink Write Printing of Resistive-Type Humidity Sensors," *Flexible and printed electronics*, **6**(4), pp. 45007-.
- [9] Hines, D. R., Gu, Y., Martin, A. A., Li, P., Fleischer, J., Clough-Paez, A., Stackhouse, G., Dasgupta, A., and Das, S., 2021, "Considerations of Aerosol-Jet Printing for the Fabrication of Printed Hybrid Electronic Circuits," *Additive Manufacturing*, **47**, p. 102325.
- [10] Cooper, C., and Hughes, B., 2020, "Aerosol Jet Printing of Electronics: An Enabling Technology for Wearable Devices," *2020 Pan Pacific Microelectronics Symposium (Pan Pacific)*, pp. 1–11.
- [11] Li, J., Wang, Y., Xiang, G., Liu, H., and He, J., 2019, "Hybrid Additive Manufacturing Method for Selective Plating of Freeform Circuitry on 3D Printed Plastic Structure," *Advanced Materials Technologies*, **4**(2), p. 1800529.
- [12] Li, J., Zhang, Y., Wang, P., Wang, G., Liu, Y., Liu, Y., and Li, Q., 2021, "Selectively Metalizable Stereolithography Resin for Three-Dimensional DC and High-Frequency Electronics via Hybrid Additive Manufacturing," *ACS Appl. Mater. Interfaces*, **13**(19), pp. 22891–22901.
- [13] Yu, Y.-Z., Lu, J.-R., and Liu, J., 2017, "3D Printing for Functional Electronics by Injection and Package of Liquid Metals into Channels of Mechanical Structures," *Materials & Design*, **122**, pp. 80–89.
- [14] Wu, S.-Y., Yang, C., Hsu, W., and Lin, L., 2015, "3D-Printed Microelectronics for Integrated Circuitry and Passive Wireless Sensors," *Microsystems & Nanoengineering*, **1**(1), p. 15013.